Molecular Insights into the Interactions between PEG Carriers and Drug Molecules from Celastrus hindsii: A Multi-scale Simulation Study

Thi H. Ho
Van Lang University
Hien Duy Tong
Vietnamese-German University
Thuat T. Trinh
thuat.trinh@ntnu.no

Norwegian University of Science and Technology

Article

Keywords:

Posted Date: June 27th, 2024

DOI: https://doi.org/10.21203/rs.3.rs-4557668/v1

Additional Declarations: No competing interests reported.

Version of Record: A version of this preprint was published at Scientific Reports on July 22nd, 2024. See the published version at https://doi.org/10.1038/s41598-024-67720-4.

Molecular Insights into the Interactions between PEG Carriers and Drug Molecules from *Celastrus hindsii*: A Multi-scale Simulation Study

Thi H. Ho[1,2], Hien Duy Tong[3], and Thuat T. Trinh[4,*]

[1]Laboratory for Computational Physics, Institute for Computational Science and Artificial Intelligence, Van Lang University, Ho Chi Minh City, 700000, Vietnam
[2]Faculty of Mechanical - Electrical and Computer Engineering, School of Technology, Van Lang University, Ho Chi Minh City, 700000, Vietnam
[3]Faculty of Engineering, Vietnamese-German University (VGU), Thu Dau Mot City, Binh Duong Province 75000, Vietnam
[4]Porelab, Department of Chemistry, Norwegian University of Science and Technology, NTNU, Trondheim, NO-7491, Norway
[*]thuat.trinh@ntnu.no

ABSTRACT

Efficient drug delivery is crucial for the creation of effective pharmaceutical treatments, and polyethylene glycol (PEG) carriers have been emerged as promising candidates for this purpose due to their bio-compatibility, enhancement of drug solubility, and stability. In this study, we utilized molecular simulations to examine the interactions between PEG carriers and selected drug molecules extracted from *Celastrus hindsii*: Hindsiilactone A, Hindsiiquinoflavan B, Maytenfolone A, and Celasdin B. The simulations provided detailed insights into the binding affinity, stability, and structural properties of these drug molecules when complexed with PEG carriers. A multi-scale approach combining Density Functional Theory (DFT), extended Tight-Binding (xTB), and Molecular Dynamics (MD) simulations was conducted to investigate both unbound and bound states of PEG/drug systems. The results from DFT and xTB calculations revealed that the unbound complex has an unfavorable binding free energy, primarily due to negative contributions of delta solvation free energy and entropy. The MD simulations provided more detailed insights into the interactions between PEG and drug molecules in water solutions. By integrating the findings from the multi-scale simulations, a comprehensive picture of the unbound and bound states of PEG and drug systems were obtained. This information is valuable for understanding the molecular mechanisms governing the binding of drugs in PEG-based delivery platforms, and it contributes to the rational design and optimization of these systems.

Introduction

Polyethylene glycol (PEG) is a widely-used polymer, applied in multiple scientific disciplines such as drug delivery systems due to its versatility[1,2]. PEGylation, the covalent attachment of PEG chains to macro molecules or nanoparticles, enhances solubility, stability, and bio compatibility, thereby improving pharmacokinetics and pharmacodynamics profiles, leading to increased efficacy and safety of therapeutic agents[1]. In drug delivery systems, PEG coating offers numerous advantages including prolonged systemic circulation time, protection against enzymatic degradation, enhanced cellular uptake, and improved targeted delivery[2]. PEGylation has been shown to enhance therapeutic efficacy of various types of drugs, including small molecules, peptides, proteins, and nucleic acids[3,4].

Molecular simulations has been a powerful tool for understanding the properties and behavior various materials[5–10] including PEG-based materials, such as polymers, nanoparticles, and hydrogels[11–14]. For instance, Lee et al.[11] found good agreement between simulated and experimental hydrodynamic radii of PEG and polyethylene oxide (PEO) polymers in water. Brambilla et al.[14] investigated the interaction between amyloid-beta peptide and long-circulating polymeric nanoparticles, suggesting potential for improved Alzheimer's disease conditions. Bunker et al.[15] reviewed the importance of molecular dynamics simulations in obtaining mechanistic insights into liposome-based drug delivery systems structure and behavior, while Magarkar et al.[16] investigated the molecular mechanism behind PEG's steric shielding effect on conjugated proteins. The latter study found that PEGylated protein binding affinity depends on chain length and location, providing valuable insights for therapeutic applications. It is crucial to recognize that the PEG polymer can form both unbound (non-covalent interactions) and bound (covalent bonding) complexes with drug molecules. The behavior of these two distinct systems in water solutions can be significantly different, as demonstrated by Li et al.[17].

Celastrus hindsii, a plant native to Vietnam, China, and Southeast Asia, has long been used traditionally for its medicinal properties and insecticidal qualities[18]. The leaves of this plant contain flavonoids, sesquiterpenes, diterpenes, triterpenes, alkaloids, and other compounds with antioxidant and antitumor activities[18]. Ly et al. isolated rosmarinic acid oligomers from the leaves of *Celastrus hindsii*, which exhibited antioxidative activity against methyl linoleate autooxidation and radical-initiated peroxidation of soybean in liposomes[19].

Furthermore, various bioactive compounds have been discovered in *Celastrus hindsii*, such as celahin D, an agarofuran sesquiterpene polyol ester was isolated by Huang et al.[20], and celahin C, another sesquiterpene ester also found in the same species[21]. Su et al. demonstrated over one hundred bioactive compounds from *Celastrus hindsii* with diverse biological activities, including anti-inflammatory, analgesic, and antitumor effects[22]. New compounds such as hindsiilactone A and hindsiiquinoflavan B[23] and maytenfolone-A[22] have also been discovered in *Celastrus hindsii*. Additionally, other compounds such as Celasdin-A, Celasdin-C, anti-AIDS Celasdin-B, and cytotoxic maytenfolone-A were identified by Kuo et al.[24]. Recently, Viet et al.[25] isolated a mixture of α-amyrin and β-amyrin with antioxidant, xanthine oxidase, and tyrosinase inhibitory potential from its leaves.

The rich phytochemical composition of *Celastrus hindsii* supports its traditional use in folk medicine and as an insecticide[18,22]. However, despite their significant pharmacological potential, the clinical applications of many bioactive compounds are often hindered by challenges related to poor solubility, low bioavailability, and limited stability[2]. To address these obstacles, effective drug delivery systems can be developed, such as those based on PEG carrier systems and PEGylation. The success of PEG-based drug delivery systems depends crucially on understanding the molecular interactions between the PEG carriers and the drug molecules of interest.

In this study, we employ molecular simulations to investigate the interaction between PEG carriers and several selected bioactive compounds derived from *Celastrus hidsii*. We investigate both the unbound system, which refers to non-covalent interactions between PEG and drug molecules, and the bound system, which denotes covalent bonding between PEG and drugs. The aim was to gain insights into the molecular-level details that govern their stability and behavior. To conduct the simulations, we utilize a combination of Density Functional Theory (DFT), extended Tight-Binding (xTB) methods, and classical molecular dynamics (MD) simulations. The results of the simulations reveal important insights into the nature of the PEG-bioactive compound interactions.

Results and Discussion

DFT calculations

The results from the DFT calculations including computation of electronic structure and binding energy are reported in this section. The Molecular Electronic Potential (MEP) is also discussed. The MEP results for drug molecules, visualized in Figure 1, indicate that HINA and HINB display greater polarization than MAYA and CELB, due to more functional groups and oxygen atoms, increasing molecular polarity. High polarization in HINA and HINB could affect interactions with PEG carriers and solvation free energy. The MEP figure for PEG.drug system (as shown in Fig S1 of the SI) follows the same trend.

As described earlier in the method sections, the optimized structures of the two lowest-energy conformers for each PEG.drug complex are presented in Figure 2. We observed that the main interactions between PEG and drug molecules are the vdW interactions between heavy atoms.

The DFT-computed binding energy and solvation free energy were summarized in Table 1. The values of binding energies (ΔE_{bind}^{DFT}) reveal favorable drug-PEG interactions for all complexes as indicated by negative values between -69 kJ/mol and -171 kJ/mol. This suggests that the PEG.drug binding is energetically favorable under the gas-phase conditions.

Table 1 also presents the solvation free energies (ΔG_{solv}^{DFT}) of the drug molecules follow the trend: HINB $>$ MAYA $>$ HINA $>$ CELB. This aligns with their MEP results, where HINB shows the highest polarity and CELB displays the lowest polarity (Figure 1). It is not surprising that PEG exhibits more favourable solvation free energies than the drug molecules due to its hydrophilic behavior[1] , which promote stronger interactions with the water solvent.

Upon comparing solvation free energies of the drug molecules and their corresponding unbound complexes with PEG carriers, we observed a significant increase in solvation free energy upon complex formation (almost three times higher for the PEG.drug complexes compared to individual drug molecules). However, determining the thermodynamics of these interactions requires considering delta solvation free energy ($\Delta\Delta G_{solv}^{DFT}$), which ranged from 17 kJ/mol to 54 kJ/mol (see Table 1). The positive values of the delta solvation free energy indicate that the solvation process is not favorable for complex formation process.

The reaction energies of the PEGylation process for the four bound PEG-drug systems, obtained through DFT calculations, are presented in Table 2. The results reveal that the formation of PEG-HINA exhibits the most favorable $\Delta E_{reaction}^{DFT}$ (-75 kJ/mol), while the formation of PEG-MAYA is unfavorable (80 kJ/mol). As demonstrated in Figure 3, the MAYA molecule forms a specific bonding position with the PEG fragment, it generally tends to have fewer contacts with the PEG chain compared to the

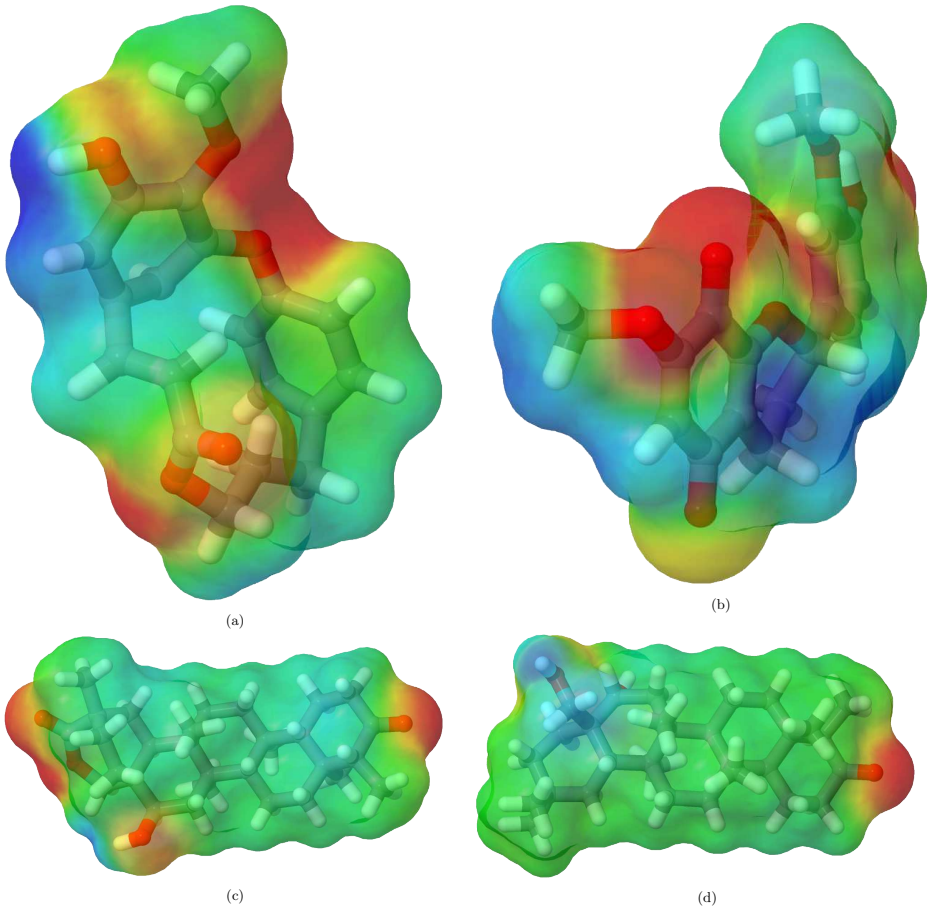

Figure 1. Visualization of Molecular Electronic Potential obtained from DFT calculations for drug molecules of HINA (a), HINB (b), MAYA (c), and CELB (d). The red color indicates regions of negative electrostatic potential, which are electron-rich areas. The blue color indicates regions of positive electrostatic potential, which are electron-deficient areas.

Table 1. Calculated bind energy (kJ/mol) and solvation free energy (kJ/mol) obtained from DFT calculation for unbound PEG.drug complexes.

System	ΔE^{DFT}_{bind}	$\Delta G^{DFT}_{solv,PEG.drug}$	$\Delta G^{DFT}_{solv,drug}$	$\Delta G^{DFT}_{solv,PEG}$	$\Delta\Delta G^{DFT}_{solv}$
PEG.HINA 1	-171	-147	-50	-150	54
PEG.HINA 2	-92	-168	-54	-132	17
PEG.HINB 1	-69	-178	-68	-147	37
PEG.HINB 2	-104	-179	-69	-147	37
PEG.MAYA 1	-124	-189	-58	-166	35
PEG.MAYA 2	-107	-179	-55	-162	38
PEG.CELB 1	-163	-160	-44	-163	47
PEG.CELB 2	-159	-166	-43	-169	47

other drug molecules. This reduced interaction may contribute to the less favorable reaction energy observed for the formation of PEG-MAYA.

The results indicate that the PEGylation reaction leading to the formation of PEG-drug is favorable for HINA, HINB, and CELB systems, while it is unfavorable for MAYA. The interaction between the drug molecule and the PEG fragment appears to be a crucial factor in determining this reaction.

xTB calculations

In this section, the xTB method was utilized to compute solvation free energies and binding energies of PEG.drug complexes. The xTB results indicate that drug molecules display significantly higher solvation free energies upon forming complexes with

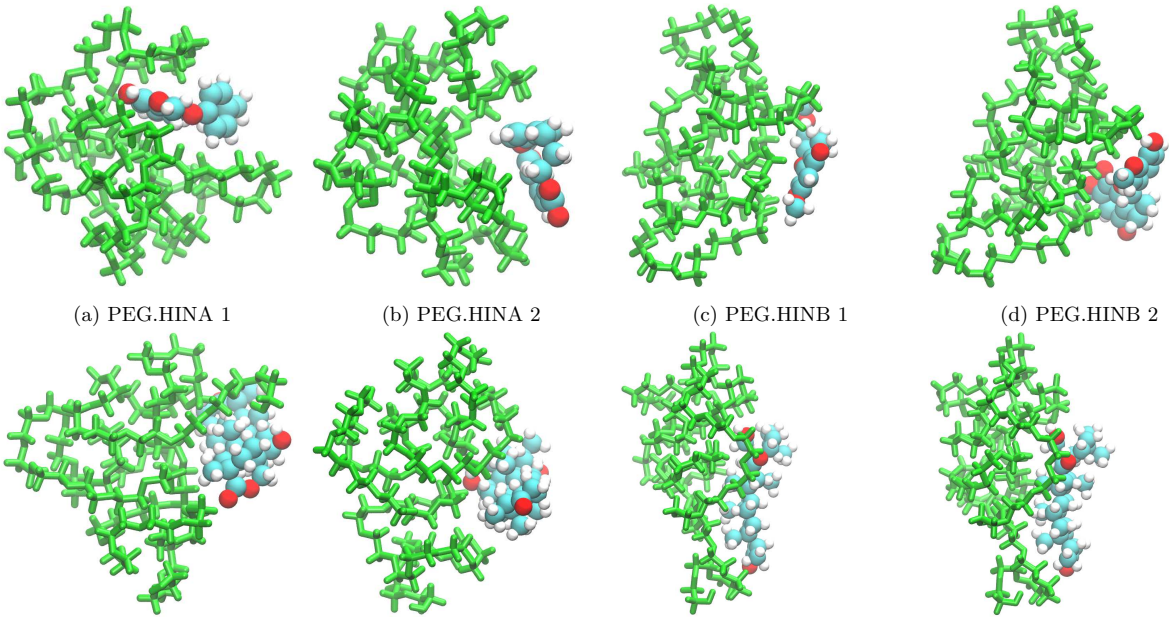

(a) PEG.HINA 1 (b) PEG.HINA 2 (c) PEG.HINB 1 (d) PEG.HINB 2

(e) PEG.MAYA 1 (f) PEG.MAYA 2 (g) PEG.CELB 1 (h) PEG.CELB 2

Figure 2. Optimized structures of unbound PEG.drug complexes obtained from DFT calculations. The PEG molecules are presented in green color for a better visualization.

Table 2. Calculated reaction energy (kJ/mol) for the PEGylation process to form covalent bonded PEG-drug molecules.

System	$\Delta E^{DFT}_{reaction}$	$\Delta E^{xTB}_{reaction}$
PEG-HINA	-75	-31
PEG-HINB	-40	-5
PEG-MAYA	80	29
PEG-CELB	-10	13

PEG carriers, consistent with the DFT findings. The solvation free energy of the complexes is approximately five times greater than that of the individual drug molecule (see Table 3). This enhancement primarily comes from PEG's favorable solvation. The difference in solvation free energy of the complexed system ($\Delta\Delta G^{xTB}_{solv}$) remains unfavorable (Table 4). The positive $\Delta\Delta G^{xTB}_{solv}$ values, ranging from 6 to 34 kJ/mol, again imply an unfavorable solvation energy for the unbound PEG.drug systems.

The binding energies ΔE^{xTB}_{bind} in Table 4 show favorable gas-phase interactions between PEG carriers and drug molecules (-113 to -72 kJ/mol). However, the entropic effects ($T\Delta S$), calculated from frequency calculations yields negative values,

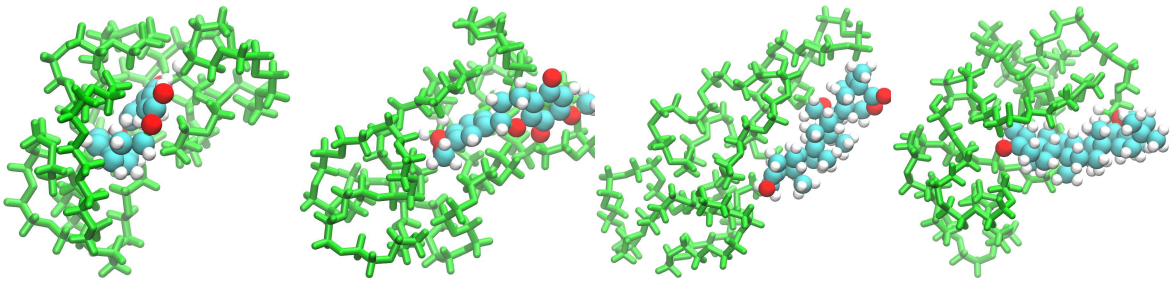

(a) PEG-HINA (b) PEG-HINB (c) PEG-MAYA (d) PEG-MAYB

Figure 3. Optimized structures of covalent bound PEG-drug molecules obtained from DFT calculations. The PEG fragments are presented in green color for a better visualization.

Table 3. Solvation free energy (kJ/mol) obtained from xTB calculations for the unbound PEG.drug systems.

System	$\Delta G^{xTB}_{solv,PEG.drug}$	$\Delta G^{xTB}_{solv,drug}$	$\Delta G^{xTB}_{solv,PEG}$
PEG.HINA 1	-303	-58	-254
PEG.HINA 2	-310	-58	-258
PEG.HINB 1	-289	-60	-234
PEG.HINB 2	-273	-60	-235
PEG.MAYA 1	-313	-67	-273
PEG.MAYA 2	-307	-66	-271
PEG.CELB 1	-278	-57	-254
PEG.CELB 2	-273	-57	-250

indicating unfavorable entropic changes during the formation of PEG.drug complex. The final binding free energy (ΔG^{xTB}_{bind}) for complexes in aqueous solution was determined using equation 3. Table 4 shows the calculated binding free energies, which are predominantly positive (between -8 to 18 kJ/mol). This suggests that complex formation is entropy-driven and may be unstable in aqueous environments, as these positive values indicate unfavorable thermodynamics for complex stability.

Table 4. Calculated binding energy, solvation free energy and binding free energy obtained from xTB calculations for unbound PEG.drug complexes. All value units are in kJ/mol.

System	ΔE^{xTB}_{bind}	$T\Delta S^{xTB}$	$\Delta\Delta G^{xTB}_{solv}$	ΔG^{xTB}_{bind}
PEG.HINA 1	-81	-64	9	-8
PEG.HINA 2	-72	-73	7	8
PEG.HINB 1	-80	-74	6	0
PEG.HINB 2	-79	-69	22	12
PEG.MAYA 1	-85	-76	26	18
PEG.MAYA 2	-89	-77	30	18
PEG.CELB 1	-102	-83	34	14
PEG.CELB 2	-113	-87	34	8

The present results highlights the significance of accounting for both thermodynamic and entropic factors when engineering drug delivery systems based on compounds derived from *Celastrus hindsii* and PEG carriers. While the binding energy between PEG and the drug compound are favorable, the substantial unfavorable entropy change and delta solvation free energy contribute to the overall instability of the complex. The findings from static and implicit water simulations provide valuable insights; however, these approaches might be limited in their ability to accurately capture the intricate interactions between PEG and the drug carrier in a more realistic aqueous environment. To verify and further elucidate these results, a series of MD simulations were conducted. These simulations have incorporated explicit water molecules, allowing for a more detailed investigation into the dynamic behavior and interaction between PEG and the drug carrier in solutions.

MD simulations

In the molecular dynamics study, we first analyzed the separation of PEG carrier and bioactive drug molecules during the simulation process. As depicted in Figure 4, which shows a typical snapshot of the last MD frame for the unbound system after 100 ns of simulations, it is evident that the PEG carrier and the drug molecule have indeed separated from each other. This observation aligns with findings reported in previous literature on the interaction between PEG and small molecules in the unbound state[17]. The MD simulations, in conjunction with previous DFT and xTB simulations, consistently demonstrate the separation of the PEG carrier and bioactive drug molecules. This observation shows the reliability and consistency of the computational methods employed in studying the behavior of these systems.

In contrast to the unbound system, when examining the bound system PEG-drug, we observe that no separation occurs after 100 ns of molecular dynamics simulations (Figure 5). This striking difference between the unbound and bound systems is attributed to the formation of chemical bonds between small molecules and PEG molecules. The establishment of these strong chemical interactions significantly enhances the overall interaction between the components, effectively preventing their dissociation from one another.

Solvent Accessible Surface Area

The solvent-accessible surface area (SASA) analysis is one of the most important properties of the PEG and small drug molecules interaction[17]. We calculated the SASA for each sampled configuration of both unbound and bound systems. By

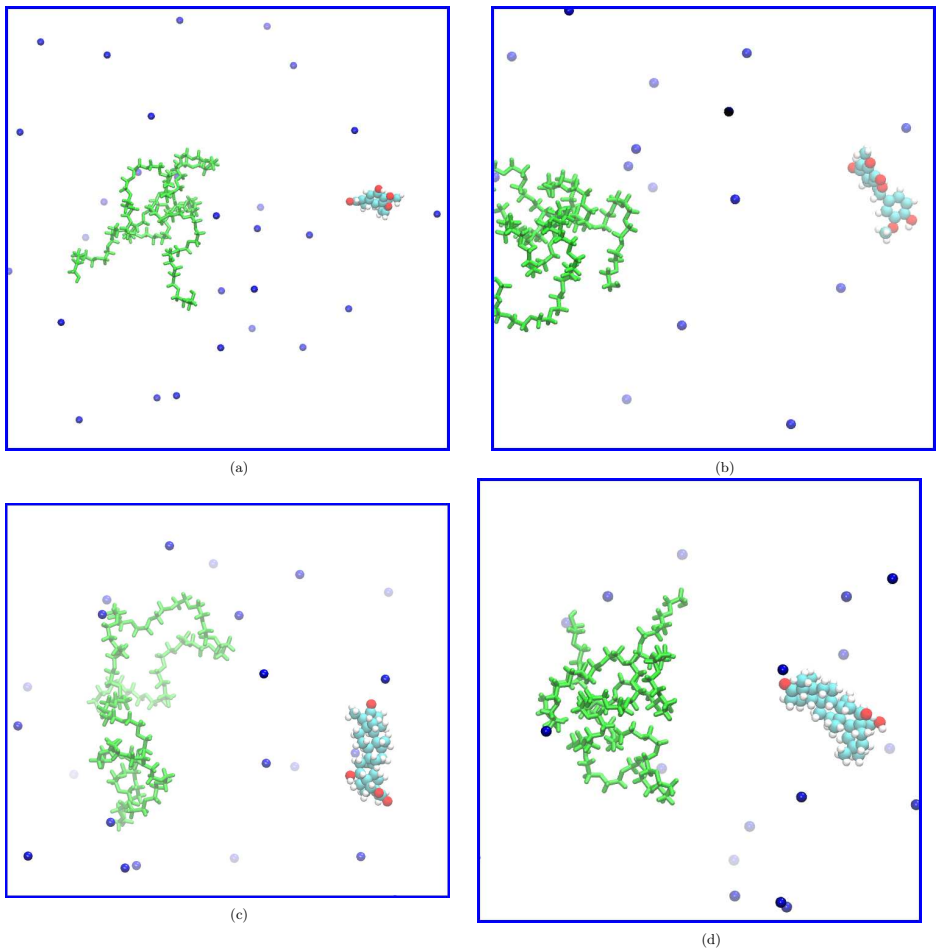

Figure 4. Representative snapshots of the last MD frame for the unbound systems after 100 ns of simulations, demonstrating the separation of the PEG carrier and the bioactive drug molecules. The green and blue colors represent the PEG and Na, respectively.

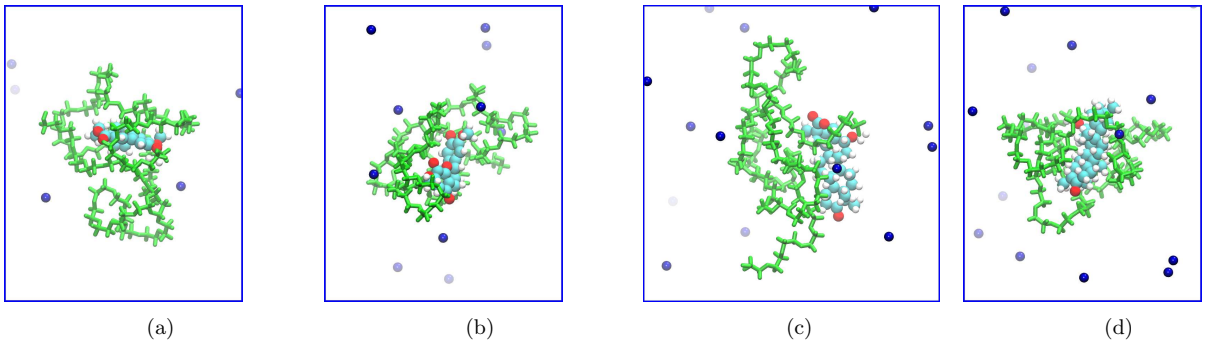

Figure 5. Representative snapshots of the last MD frame for the bound systems after 100 ns of simulations, demonstrating no separation between the PEG carrier and the bioactive drug molecules due to the formation of chemical bonds. The green and blue colors represent the PEG and Na, respectively.

determining the portion of a molecule's surface area covered by PEG, we gained insights into their dynamic molecular mechanisms. The SASA calculations included assessing total surface areas and interactions with the PEG polymer, considered as a part of the solvent. Combining results from all sampled configurations in histograms (Figure 6) revealed trends and patterns on how these compounds interact during the simulations.

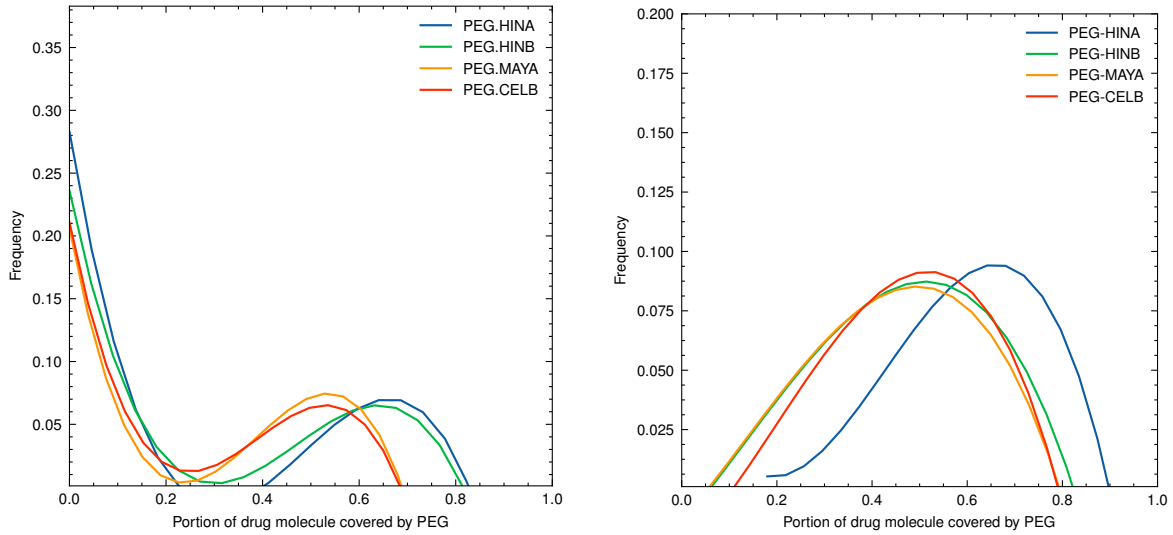

(a) Unbound **(b)** Bound

Figure 6. Histograms of the fraction of drug surface covered by PEG for unbound (a) and bound (b) systems.

In the unbound systems, we observed that there was generally no significant interaction between the PEG carrier and bioactive drug molecules from *Celastrus hindsii* for most of the simulation time. Consequently, the coverage by PEG over these compounds remained at very low portion (< 0.2) for a majority of the sampling configurations (See Figure 6.a). However, a distinct peak is observed for PEG coverage at a very low frequency. This indicates that during the MD simulation, the PEG carrier and drug molecule only interact in a very small fraction of simulation time. Furthermore, we found that the PEG coverage for the unbound systems involving PEG.HINA and PEG.HINB were approximately 0.65, while those with PEG.MAYA and PEG.CELB exhibited coverage values of around 0.55. This difference in PEG coverage can be attributed to the size disparities between HINA/HINB and MAYA/CELB molecules. Smaller molecules tend to have a higher coverage percentages with the PEG carrier, which may influence their overall behavior within the PEG-based drug delivery system.

In constranst, bound systems displayed a significantly different behavior compared to unbound systems, with PEG effectively covering the bioactive drug molecules from *Celastrus hindsii* most of the time. The absence of low portion peak and a wider PEG coverage range (0.1-0.9) in the histogram data confirmed that chemical bonds favored the interaction between PEG and drug molecules in solutions (See Figure 6.b). In the unbound system, the highest frequency is observed around 0.0 for PEG coverage, indicating that the unbound compounds tend to be separated. However, the bound system exhibits a peak of high frequency at approximately 0.5, suggesting that in the bound state, the compounds are more closely associated, leading to higher PEG coverage values. This observation highlights the potential benefits of PEGylation for enhanced PEG coverage and for protection of the small drug molecules.

To further investigate the conformational behaviour of the bound compounds, additional calculations on another conformer of the bound systems, PEG-drug 2, were performed (see SI). The results (Table S1) show that the xTB-calculated relative energy of the PEG-drug 2 system is higher than that of the PEG-drug system. Due to the high computational cost of the DFT method, we did not perform the DFT calculations for the PEG-drug 2 systems. The SASA analysis from the MD simulations of the PEG-drug 2 conformer (See SI) exhibits a similar pattern as observed for the PEG-drug systems. This indicates that the drug molecule in this conformation also experiences increased PEG coverage when bound to the PEG carrier.

Radius of gyration

We also calculated the radius of gyration (Rg) for PEG molecules in both unbound and bound configurations to supplement the SASA analysis. The results demonstrated that there was no significant difference observed between the Rg values for PEG in solution and those encountered within the unbound system simulations (see Figure 7). These findings were consistent with previous molecular dynamics studies on similar PEG-based systems[17], further validating the accuracy of the methodology. The

average Rg value obtained for PEG molecules across all unbound systems was approximately 0.85 nm, which in excellent agreement with previous study[17].

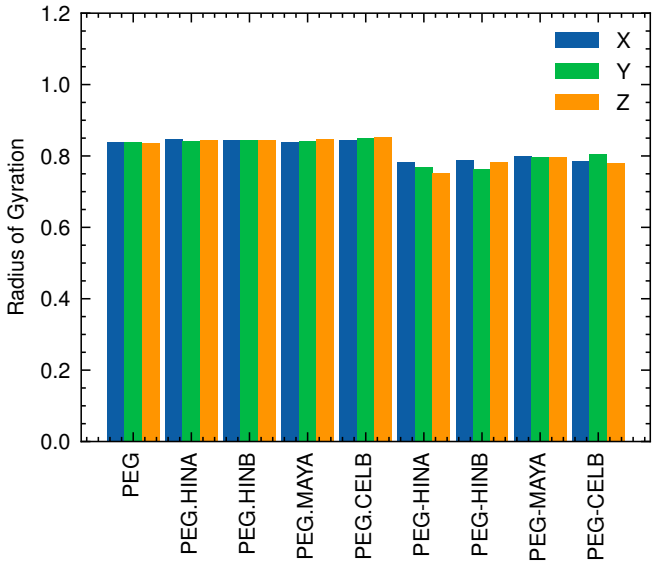

Figure 7. x, y, z components of the radius of gyration of PEG molecule in both unbound (PEG.drug) and bound (PEG-drug) systems.

In contrast to the findings for unbound systems, we observed a reduction in the Rg values (around 0.77 nm) for PEG carrier when bound with bioactive drug molecules. This observation suggests that an attractive nonbonded interaction may be occurring between the PEG and these compounds, causing the PEG polymer reducing the Rg.

Discussion

In this section, we will compare and contrast the performance of the xTB and DFT methods in the context of investigating PEG-drug interactions. The xTB approach is known for its computational efficiency and lower accuracy compared to DFT[26]. Despite its limitations, xTB can serve as a useful tool for providing preliminary insights into the behavior of complex systems. Here, we aim to assess the level of agreement between the results obtained from xTB and DFT calculations for PEG-drug interactions. This comparison will help us understand the reliability of xTB in predicting the binding energy and solvation free energy of these complexes.

As depicted in Figure 8, we observed that the xTB method can capture the trend of the DFT calculations regarding the binding energy between PEG and drug molecules. However, the DFT-calculated binding energies were more negative than the corresponding xTB-calculated binding energies, which suggests a stronger binding interaction between the PEG and drug molecules in the case of DFT calculations. While it would be ideal to compare these values with experimental data, to the best of our knowledge, there are no available experimental data or other DFT data for the binding energy of these specific complexes.

The delta solvation free energy is a critical component of the overall binding free energy for PEG-drug complexes. The analysis showed that the level of agreement between the xTB and DFT methods was notably weaker when examining the delta solvation free energies, as demonstrated in Figure 8.b. The linear regression's coefficient of determination (R^2) for this comparison is only 0.13, which indicates a very low correlation between these methods. This discrepancy can be attributed to the less accurate auxiliary basis method employed in xTB and the ALPB model when compared to more sophisticated solvation techniques available in VASP software for DFT-based calculations. This observation underscores the importance of considering both binding and solvation free energies in evaluating computational methods for predicting PEG-drug interactions, as well as highlights the limitations of xTB when it comes to solvation free energy calculations relative to DFT. However, it is important to note that despite its limitations, xTB remains a valuable tool for providing preliminary insights into large and complex systems due to its computational efficiency.

While both the xTB and DFT methods, when employed using static calculations, provide valuable insights into the structural properties and binding affinity of PEG.drug complexes, they do not account for the dynamic behavior of these systems at finite temperatures or their explicit interactions with water solvent molecules. This limitation can result in an incomplete picture of the forces governing the formation and stability of these complexes. The MD approach, on the other hand, offers a more

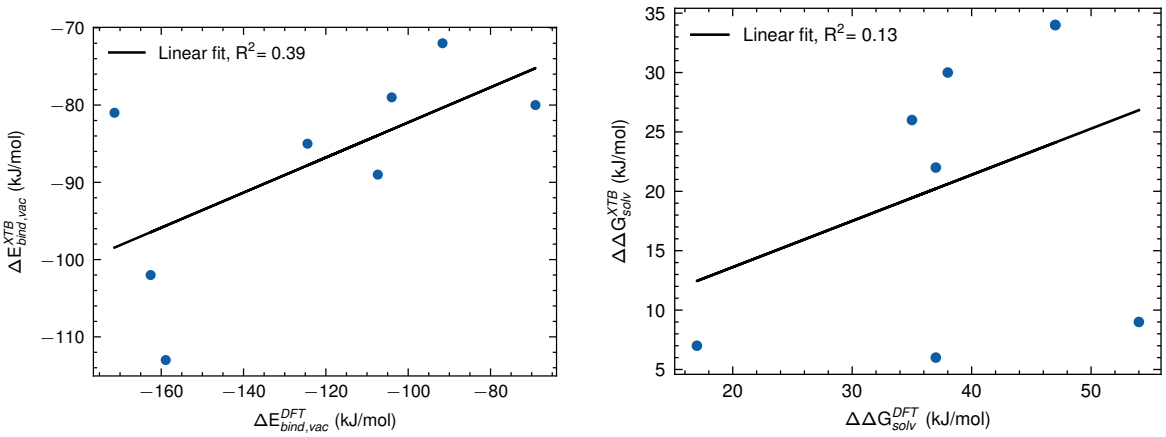

(a) Binding energy

(b) Delta solvation free energy

Figure 8. Comparison of calculated values obtained from DFT and xTB calculations for binding energy (a) and for delta solvation free energy (b).

dynamic perspective by simulating the system's behavior at finite temperatures and accounting for the explicit interactions with solvent molecules. This enabled us to observe how the intricate interactions between water and PEG-drug systems influence their overall properties. For instance, we discovered that the majority of the time, there is no interaction between PEG and drug molecules in unbound configurations, which aligns well with the less favorable binding energies calculated using DFT simulations.

It is important to note that while the MD simulations offer valuable insights into the dynamic behavior of PEG-drug complexes, they also come with their own limitations, such as the need for accurate force fields and the computational cost associated with long simulations[15]. Therefore, it is essential to carefully consider the appropriate level of theory and simulation methods when studying these systems.

Conclusions

The study utilized a multi-scale computational approach that combined DFT, xTB , and molecular dynamics simulations to examine the interaction between polyethylene glycol (PEG) carrier systems and bioactive drugs derived from *Celastrus hindsii*. By examining the binding energies, solvation free energies, and dynamic interactions in both bound and unbound states, we gained insights into these complex molecular processes.

The simulations revealed that both the DFT and xTB methods predicted unfavorable binding free energies for the PEG-drug system. This can be attributed to delta solvation free energy and entropy considerations. The entropic penalty of confining the PEG.drug complexes outweighing any gains in binding energy. Unfavorable solvation free energies of the complexation process may also drive these interactions towards less stable configurations. Therefore, researchers should consider these factors in formulating effective pharmaceutical products using PEG-based nanocarriers loaded with bioactive compounds.

The results from MD simulations suggest that PEG carrier and the small drug molecules rarely interact in unbound configurations, consistent with previous findings on PEG-based systems with small drug molecules[17]. This work also indicates that the PEGylation of drug molecules increases stability compared to unbound systems. The strengthening of interactions between small molecules and the PEG molecule, attributed to the formation of chemical bonds, contributes to this enhanced stability. The solvent-accesible surface area analysis confirmed the presence of PEG coverage on drug molecules during specific time periods, highlighting the potential for PEG-based nanocarriers to improve the solubility and bioavailability of the drug molecules.

While the MD simulations in this study represent the first attempt to explore the behavior of the PEG-drug complex in water and the effects of covalent bonding, they cannot directly address the drug release mechanism in a realistic environment due to the inherent limitations of classical force fields. Accurate simulation of drug release, including chemical bond breaking and forming, would require more advanced methods such as ab initio molecular dynamics (AIMD).

It is important to note that while this study provides valuable insights into the interactions between PEG carrier systems and bioactive drugs derived from *Celastrus hindsii*, further experimental studies are needed to validate these findings and assess their implications for the design and optimization of PEG-based delivery platforms. Additionally, further investigation could focus on the chemical activity of PEGylated drug molecules and the kinetics of the PEGylation process, including compound

association/dissociation rates. A deeper understanding of these dynamics could lead to enhanced control over drug release profiles and increased therapeutic potential of PEG-based nanocarriers loaded with the bioactive compounds.

Models and Methods

Models

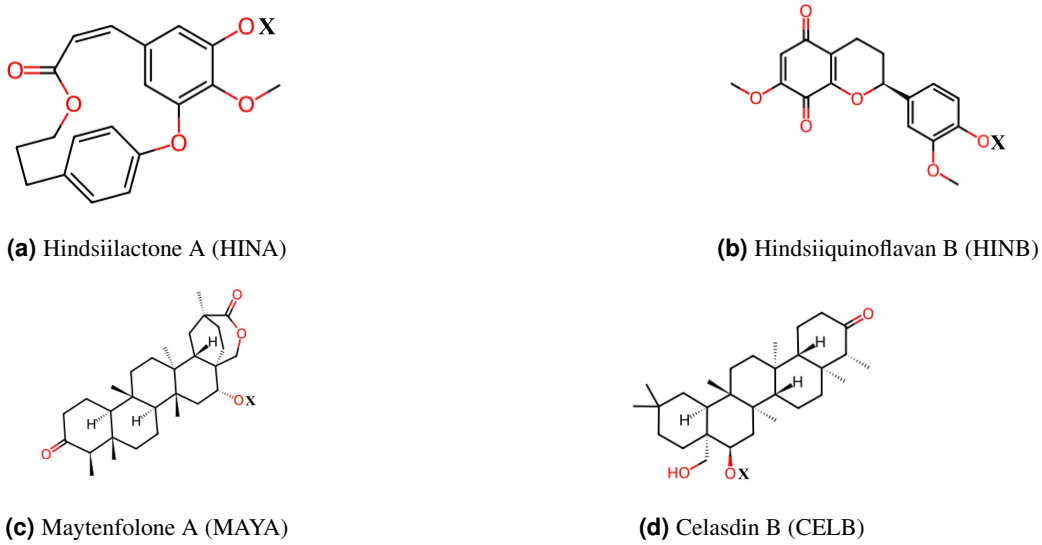

(a) Hindsiilactone A (HINA)

(b) Hindsiiquinoflavan B (HINB)

(c) Maytenfolone A (MAYA)

(d) Celasdin B (CELB)

Figure 9. Chemical structures of selected bioactive compounds from *Celastrus hindsii* in this study. Illustration of unbound complexes (X = H) and bound PEG-drug molecule with PEG chain (X = PEG) for a better visualization of binding positions.

The chemical structures of selected bioactive compounds are presented in Figure 9. We adopted a concise notation to represent the chemical structures of the drug molecules. For clarity and brevity throughout the manuscript, we refer to these compounds as HINA (Hindsiilactone A), HINB (Hindsiiquinoflavan B), MAYA (Maytenfolone A), and CELB (Celasdin B). The PEG molecule was the 45 monomer unit linear chain polymer, also known as PEG2000[1,2].

We modeled both unbound and bound states between PEG and drug molecules. In the unbound state (X = H in Figure 9), initial interactions are dominated by van der Waals (vdW) forces, with no covalent bonding (PEG and drug molecules exist as separate entities). This contrasts with bound state interactions where bonding occurs between PEG carriers and drug molecules, stabilizing the complex (X = PEG in Figure 9).

Methods

To understand the interactions between PEG carriers and drug molecules, we utilized DFT, xTB and MD simulations. These techniques offered insights into the binding properties, electronic structure, and overall behavior of the PEG-drug complexes, enabling investigation of their potential in drug delivery systems. By combining results from these various simulation methods, a comprehensive understanding of the interactions between PEG carriers and *Celastrus hindsii*'s bioactive compounds was achieved.

DFT calculations were conducted using the Vienna ab initio simulation package (VASP)[27,28] with the projected augmented wave (PAW) pseudo-potential method[29]. The generalized gradient approximation Perdew-Burke-Ernzerhof functional (PBE)[30] was used for exchange-correlation effects, and the semi-empirical DFT-D2 dispersion correction method[31] was employed to treat van der Waals interactions. A 400 eV cutoff energy, Γ point Brillouin zone summation with Gaussian broadening of 0.1 eV. The selected simulation box, with a 30 Å x 30 Å x 30 Å cubic cell and a 10-15 Å vacuum layer surrounding the PEG-drug complex, ensures that self-interactions between periodic images are minimized while maintaining reasonable computational efficiency. The molecules were placed in the center, fully relaxed until forces were below 0.01 eV/Å, and single-point calculations for isolated and complex systems yielded interaction energy and charge density analysis through Bader charge analysis method[32]. We employed the implicit solvation model implemented in the VASPSol package[33,34] to calculate the solvation free energies of PEG and drugs molecules.

The extended tight-binding (xTB)[26,35] method is a semi-empirical quantum chemistry approach employed in DFT simulations, striking a balance between computational efficiency and accuracy. This approach makes it particularly well-suited for investigating large systems that would be computationally costly to simulate with full DFT methods[35]. In xTB simulations, we

employed GFN2-xTB method[26,35] for studying the interaction between PEG carriers and drug molecules. The xTB method was used to optimize initial system structures, calculate frequency and solvation free energy. The solvation free energy was computed using the Analytical Linearized Poisson-Boltzmann (ALPB) model, offering insights into complexes' behavior in aqueous environments and their interaction strength affected by solvation.

Binding energy is an essential concept in understanding the interaction between PEG and a drug molecules. It refers to the energy released when the two components combine to form a complex, which can provide insights into the strength and stability of their association. The binding energy (ΔE_{bind}) between the PEG carrier and drug molecule can be represented by the following equation:

$$\Delta E_{bind} = E_{PEG.drug,opt} - (E_{PEG,opt} + E_{drug,opt}) \tag{1}$$

where $E_{\text{PEG.drug,opt}}$ is the energy of the PEG.drug complex, $E_{\text{PEG,opt}}$ and $E_{\text{drug,opt}}$ are the isolated energies of the PEG carrier and drug molecule, respectively.

In addition to the binding energy, it is also important to consider the binding free energy (ΔG_{bind}) of the complex formation[36]. This value takes into account not only the binding energy but also the changes in solvation free energy and entropy as the following equation:

$$\Delta G_{bind} = \Delta E_{bind} + \Delta\Delta G_{solv} - T\Delta S = \Delta H_{bind} - T\Delta S \tag{2}$$

where ΔH_{bind} is the enthalpy change upon complexation, T is the absolute temperature, and ΔS is the entropy change. A negative value for ΔG_{bind} indicates a favorable and stable interaction between the PEG carrier and drug molecule. The term $\Delta\Delta G_{solv}$ represents the difference in solvation free energy between the PEG-drug complex and the sum of the solvation free energies of the individual components:

$$\Delta\Delta G_{solv} = \Delta G_{solv,PEG.drug} - (\Delta G_{solv,drug} + \Delta G_{solv,PEG}) \tag{3}$$

The PEGylation reaction between PEG and drug to form bound molecules and water is described as:

$$\text{PEG} + \text{drug} = \text{PEG}{-}\text{drug} + \text{H}_2\text{O} \tag{4}$$

The PEGylation reaction energy (ΔE_{react}) was calculated as:

$$\Delta E_{react} = (E_{PEG-drug} + E_{water}) - (E_{PEG} + E_{drug}) \tag{5}$$

where $E_{PEG-drug}$, E_{water}, E_{PEG}, and E_{drug} are the total energies of the bound PEG-drug, water, free PEG, and free drug molecules, respectively.

The MD simulations employed the OPLS-AA force field[37] for PEG and drug molecules, with TIP3P water models[38]. The success of the OPLS-AA force field in previous studies on PEG thermodynamics[39] and small drug interactions[17] supports this choice. The Desmond software[40] was used for the MD simulations. The time step was set to 2 fs and the simulations were conducted at 310 K temperature, 1 bar pressure, and under the physiological conditions (0.15 M NaCl). The Isothermal-Isobaric ensemble (NPT) was used. The Lennard-Jones interactions were cut off at 1.0 nm. After reaching equilibrium for 20 ns, each simulation ran for 100 ns, repeated across 3-5 replicates. Following completion of MD simulations for both bound and unbound systems, we analyzed PEG.drug molecular interactions by calculating the radius of gyration and the solvent-accessible surface area (SASA).

Starting with the initial 3D coordinates of the drug molecule retrieved from the PubChem database[41], we performed a thorough geometry optimization using both xTB and DFT methods to refine its structure prior to molecular dynamics simulations. Initial PEG-drug complexes were constructed by positioning one drug molecule alongside one PEG chain for each compound (HINA, HINB, MAYA, and CELB), with an initial intermolecular distance of 5 Å. Subsequent geometry optimization was performed using the OPLS-AA force field. After complex formation, short-duration MD simulations were run for initial relaxation and conformational adjustment. For each unbound structure, we selected the two lowest-energy conformers as the initial structures. For the covalent bound PEG-drug complexes, only the lowest-energy conformer was selected. These conformers were then used for further calculations with the xTB and DFT methods.

In the unbound systems, we selected two conformers from DFT simulations for PEG and drug complexes, namely PEG.drug 1 and PEG.drug 2. For the bound systems, only one conformer was chosen (PEG-drug) for each drug. The details of the MD simulations are presented in Table 5. Figure 10 illustrates a snapshot of the equilibrated system PEG.HINA 1 in MD simulation.

Table 5. Details of MD simulations used in this study including the number of NaCl (N_{NaCl}), the number of water molecules (N_{water}), the total number of atoms (N_{atoms}), the box size (Å) and the simulation time.

System	N_{NaCl}	N_{water}	N_{atoms}	Box size (Å)	Simulation time
PEG	30	10776	32706	69.409	3 x 100 ns
PEG.HINA 1	30	10759	32697	69.506	5 x 100 ns
PEG.HINB 1	30	10754	32679	69.398	3 x 100 ns
PEG.MAYA 1	30	10733	32657	69.453	3 x 100 ns
PEG.CELB 1	30	10737	32672	69.352	3 x 100 ns
PEG.HINA 2	30	10768	32724	69.487	3 x 100 ns
PEG.HINB 2	30	10762	32703	69.378	3 x 100 ns
PEG.MAYA 2	30	10747	32699	69.585	3 x 100 ns
PEG.CELB 2	30	10742	32687	69.341	3 x 100 ns
PEG-HINA	30	10755	32682	69.353	5 x 100 ns
PEG-HINB	30	10756	32682	69.483	3 x 100 ns
PEG-MAYA	30	10737	32666	69.425	3 x 100 ns
PEG-CELB	30	10726	32636	69.262	3 x 100 ns

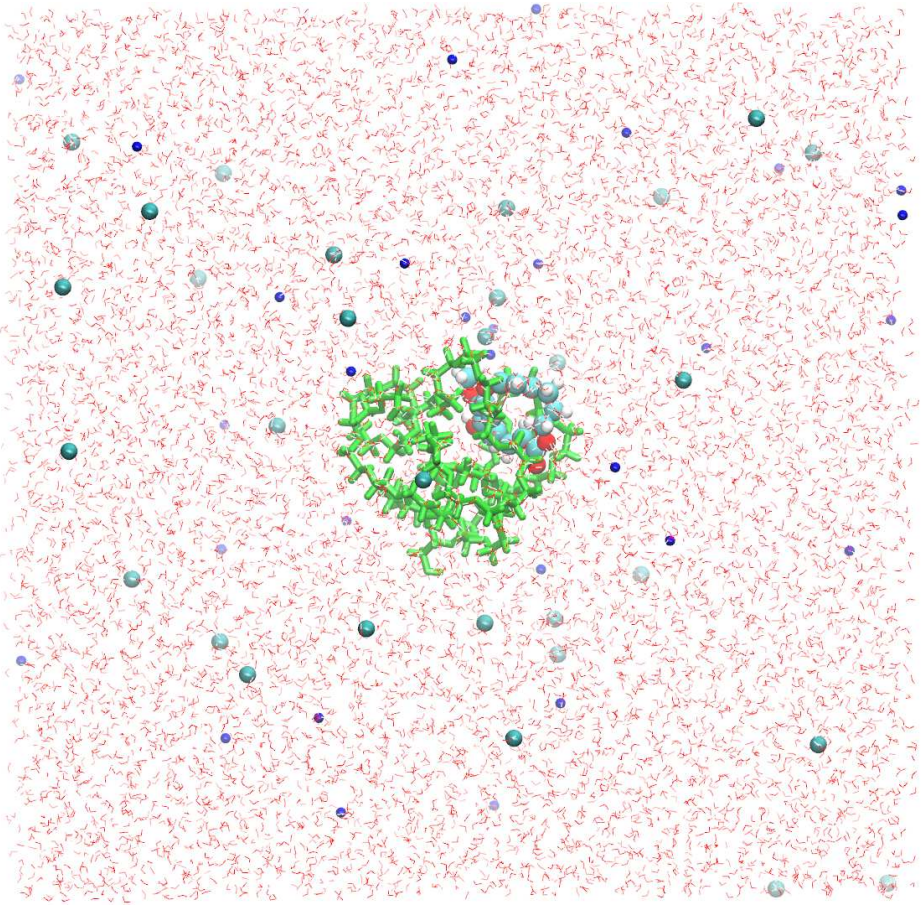

Figure 10. Snapshot of the system PEG.HINA 1 at the beginning of MD simulations. The PEG molecule depicted in green and water represented by red sticks for enhanced visual clarity.

Data availability

The datasets generated and/or analyzed during the current study are available from the corresponding author on reasonable request.

References

1. Harris, J. M. & Chess, R. B. Effect of pegylation on pharmaceuticals. *Nat Rev Drug Discov* **2**, 214–221, DOI: 10.1038/nrd1033 (2003).
2. Suk, J. S., Xu, Q., Kim, N., Hanes, J. & Ensign, L. M. PEGylation as a strategy for improving nanoparticle-based drug and gene delivery. *Adv. Drug Deliv. Rev.* **99**, 28–51, DOI: 10.1016/j.addr.2015.09.012 (2016).
3. Allen, T. M. & Cullis, P. R. Liposomal drug delivery systems: From concept to clinical applications. *Adv. Drug Deliv. Rev.* **65**, 36–48, DOI: 10.1016/j.addr.2012.09.037 (2013).
4. Liu, Z., Robinson, J. T., Sun, X. & Dai, H. PEGylated nanographene oxide for delivery of water-insoluble cancer drugs. *J. Am. Chem. Soc.* **130**, 10876–10877, DOI: 10.1021/ja803688x (2008).
5. Voter, A. F., Montalenti, F. & Germann, T. C. Extending the time scale in atomistic simulation of materials. *Annu. Rev. Mater. Res.* **32**, 321–346, DOI: 10.1146/annurev.matsci.32.112601.141541 (2002).
6. Stukowski, A. Structure identification methods for atomistic simulations of crystalline materials. *Model. Simul. Mater. Sci. Eng.* **20**, 045021, DOI: 10.1088/0965-0393/20/4/045021 (2012).
7. Wang, W. Recent advances in atomic molecular dynamics simulation of intrinsically disordered proteins. *Phys. Chem. Chem. Phys.* **23**, 777–784, DOI: 10.1039/d0cp05818a (2021).
8. Wu, J. *et al.* Mechanical instability of monocrystalline and polycrystalline methane hydrates. *Nat Commun* **6**, 8743, DOI: 10.1038/ncomms9743 (2015).
9. Ho, T. H., Do, T. H., Tong, H. D., Meijer, E. J. & Trinh, T. T. The role of chloride ion in the silicate condensation reaction from ab initio molecular dynamics simulations. *J. Phys. Chem. B* **127**, 7748–7757, DOI: 10.1021/acs.jpcb.3c04256 (2023).
10. Do, T. H., Tong, H. D., Tran, K.-Q., Meijer, E. J. & Trinh, T. T. Insight into the role of excess hydroxide ions in silicate condensation reactions. *Phys. Chem. Chem. Phys.* **25**, 12723–12733, DOI: 10.1039/d3cp00475a (2023).
11. Lee, H., Venable, R. M., MacKerell, A. D. & Pastor, R. W. Molecular dynamics studies of polyethylene oxide and polyethylene glycol: Hydrodynamic radius and shape anisotropy. *Biophys. J.* **95**, 1590–1599, DOI: 10.1529/biophysj.108.133025 (2008).
12. Li, Y., Kröger, M. & Liu, W. K. Shape effect in cellular uptake of PEGylated nanoparticles: Comparison between sphere, rod, cube and disk. *Nanoscale* **7**, 16631–16646, DOI: 10.1039/c5nr02970h (2015).
13. Li, Y., Kröger, M. & Liu, W. K. Endocytosis of PEGylated nanoparticles accompanied by structural and free energy changes of the grafted polyethylene glycol. *Biomaterials* **35**, 8467–8478, DOI: 10.1016/j.biomaterials.2014.06.032 (2014).
14. Brambilla, D. *et al.* PEGylated nanoparticles bind to and alter amyloid-beta peptide conformation: Toward engineering of functional nanomedicines for Alzheimer's disease. *ACS Nano* **6**, 5897–5908, DOI: 10.1021/nn300489k (2012).
15. Bunker, A., Magarkar, A. & Viitala, T. Rational design of liposomal drug delivery systems, a review: Combined experimental and computational studies of lipid membranes, liposomes and their PEGylation. *Biochimica et Biophys. Acta (BBA) - Biomembr.* **1858**, 2334–2352, DOI: 10.1016/j.bbamem.2016.02.025 (2016).
16. Magarkar, A., Karakas, E., Stepniewski, M., Róg, T. & Bunker, A. Molecular dynamics simulation of PEGylated bilayer interacting with salt ions: A model of the liposome surface in the bloodstream. *J. Phys. Chem. B* **116**, 4212–4219, DOI: 10.1021/jp300184z (2012).
17. Li, Y.-C. *et al.* Study of interaction between PEG carrier and three relevant drug molecules: Piroxicam, paclitaxel, and hematoporphyrin. *J. Phys. Chem. B* **116**, 7334–7341, DOI: 10.1021/jp300301z (2012).
18. Pham, D.-C. *et al.* Optimization of ultrasound-assisted extraction of flavonoids from Celastrus hindsii leaves using response surface methodology and evaluation of their antioxidant and antitumor activities. *Biomed Res. Int.* **2020**, 1–9, DOI: 10.1155/2020/3497107 (2020).
19. Ly, T. N., Shimoyamada, M. & Yamauchi, R. Isolation and characterization of rosmarinic acid oligomers in Celastrus hindsii Benth leaves and their antioxidative activity. *J. Agric. Food Chem.* **54**, 3786–3793, DOI: 10.1021/jf052743f (2006).
20. HUANG, H.-C., SHEN, C.-C., CHEN, C.-F., WU, Y.-C. & KUO, Y.-H. A novel agarofuran sesquiterpene, celahin d from celastrus hindsii BENTH. *CHEMICAL & PHARMACEUTICAL BULLETIN* **48**, 1079–1080, DOI: 10.1248/cpb.48.1079 (2000).
21. Kuo, Y.-H. *et al.* A sesquiterpene ester from celastrus hindsii. *Phytochemistry* **41**, 549–551, DOI: 10.1016/0031-9422(95)00588-9 (1996).

22. Su, X. *et al.* Chemical and pharmacological studies of the plants from genus Celastrus. *Chem. & Biodivers.* **6**, 146–161, DOI: 10.1002/cbdv.200700403 (2009).

23. Hu, X.-Q. *et al.* A new macrocyclic lactone and a new quinoflavan from celastrus hindsii. *Phytochem. Lett.* **7**, 169–172, DOI: 10.1016/j.phytol.2013.11.015 (2014).

24. Kuo, Y. H. & Kuo, L. M. Y. Antitumour and anti-AIDS triterpenes from celastrus hindsii. *Phytochemistry* **44**, 1275–1281, DOI: 10.1016/s0031-9422(96)00719-4 (1997).

25. Viet, T. D., Xuan, T. D. & Anh, L. H. α-amyrin and β-amyrin isolated from celastrus hindsii leaves and their antioxidant, anti-xanthine oxidase, and anti-tyrosinase potentials. *Molecules* **26**, 7248, DOI: 10.3390/molecules26237248 (2021).

26. Bannwarth, C., Ehlert, S. & Grimme, S. GFN2-xTB—an accurate and broadly parametrized self-consistent tight-binding quantum chemical method with multipole electrostatics and density-dependent dispersion contributions. *J. Chem. Theory Comput.* **15**, 1652–1671, DOI: 10.1021/acs.jctc.8b01176 (2019).

27. Kresse, G. & Hafner, J. Ab initio molecular dynamics for liquid metals. *Phys. Rev. B* **47**, 558 (1993).

28. Kresse, G. & Furthmüller, J. Efficiency of ab-initio total energy calculations for metals and semiconductors using a plane-wave basis set. *Comput. Mater. Sci.* **6**, 15–50, DOI: 10.1016/0927-0256(96)00008-0 (1996).

29. Kresse, G. & Joubert, D. From ultrasoft pseudopotentials to the projector augmented-wave method. *Phys. Rev. B* **59**, 1758–1775, DOI: 10.1103/physrevb.59.1758 (1999).

30. Perdew, J. P., Burke, K. & Ernzerhof, M. Generalized gradient approximation made simple. *Phys. Rev. Lett.* **77**, 3865–3868, DOI: 10.1103/physrevlett.77.3865 (1996).

31. Grimme, S. Semiempirical GGA-type density functional constructed with a long-range dispersion correction. *J Comput. Chem* **27**, 1787–1799, DOI: 10.1002/jcc.20495 (2006).

32. Tang, W., Sanville, E. & Henkelman, G. A grid-based bader analysis algorithm without lattice bias. *J. Phys.: Condens. Matter* **21**, 084204, DOI: 10.1088/0953-8984/21/8/084204 (2009).

33. Mathew, K., Sundararaman, R., Letchworth-Weaver, K., Arias, T. & Hennig, R. G. Implicit solvation model for density-functional study of nanocrystal surfaces and reaction pathways. *The J. Chem. Phys.* **140**, 084106, DOI: 10.1063/1.4865107 (2014).

34. Mathew, K., Kolluru, V. C., Mula, S., Steinmann, S. N. & Hennig, R. G. Implicit self-consistent electrolyte model in plane-wave density-functional theory. *The J. Chem. Phys.* **151**, 234101, DOI: 10.1063/1.5132354 (2019).

35. Bannwarth, C. *et al.* Extended <scp>tight-binding</scp> quantum chemistry methods. *WIREs Comput. Mol Sci* **11**, –, DOI: 10.1002/wcms.1493 (2020).

36. Gundelach, L., Fox, T., Tautermann, C. S. & Skylaris, C.-K. Protein–ligand free energies of binding from full-protein DFT calculations: Convergence and choice of exchange–correlation functional. *Phys. Chem. Chem. Phys.* **23**, 9381–9393, DOI: 10.1039/d1cp00206f (2021).

37. Jorgensen, W. L. & Tirado-Rives, J. The OPLS [optimized potentials for liquid simulations] potential functions for proteins, energy minimizations for crystals of cyclic peptides and crambin. *J. Am. Chem. Soc.* **110**, 1657–1666, DOI: 10.1021/ja00214a001 (1988).

38. Jorgensen, W. L., Chandrasekhar, J., Madura, J. D., Impey, R. W. & Klein, M. L. Comparison of simple potential functions for simulating liquid water. *The J. Chem. Phys.* **79**, 926–935, DOI: 10.1063/1.445869 (1983).

39. Hoffmann, M. M. *et al.* On the behavior of the ethylene glycol components of polydisperse polyethylene glycol PEG200. *J. Phys. Chem. B* **127**, 1178–1196, DOI: 10.1021/acs.jpcb.2c06773 (2023).

40. Bowers, K. J. *et al.* Scalable algorithms for molecular dynamics simulations on commodity clusters. In *ACM/IEEE SC 2006 Conference (SC'06)*, 84–es, DOI: 10.1109/sc.2006.54 (IEEE, 2006).

41. Kim, S. *et al.* Pubchem substance and compound databases. *Nucleic Acids Res.* **44**, D1202–D1213, DOI: 10.1093/nar/gkv951 (2016).

Acknowledgements

This work was supported by Van Lang University, Vietnamese-German University, Norwegian University of Science and Technology. T.T.T. acknowledge funding from the Research Council of Norway (RCN), the Center of Excellence Funding Scheme, Project No. 262644, PoreLab.

Author contributions statement

All authors contributed to the study conception and design. Material preparation, data collection and analysis were performed by T.H.H., T.D.H., and T.T.T. The first draft of the manuscript was written by T.H.H. and all authors commented on previous versions of the manuscript. All authors read and approved the final manuscript.

Competing interests

The authors declare no competing interests.

Additional information

Supplementary Information (SI) is available to provide additional details of the Molecular Electronic potential (MEP) maps of selected PEG.drug complexes, addition simulations of another conformer of bound system PEG-drug 2. The optimized structure, relative energy, and drug surface coverage for these systems are also provided.

Supplementary Files

This is a list of supplementary files associated with this preprint. Click to download.

- SImain.pdf